MDPI

Article

Effect of Shear Keys on the Quasi-Isolated Behavior of Small-to-Medium-Span Girder Bridges

Kefeng Yue [1], Lueqin Xu [1,2,*], Lei Fan [1], Jie Liu [1] and Hao Luo [3]

[1] School of Civil Engineering, Chongqing Jiaotong University, Chongqing 400074, China; ykf204732@163.com (K.Y.); 2420705341@163.com (L.F.); 630782447@163.com (J.L.)

[2] State Key Laboratory of Mountain Bridge and Tunnel Engineering, Chongqing Jiaotong University, Chongqing 400074, China

[3] Greentown Architecture Design, Chongqing 401121, China; haoluo000@outlook.com

* Correspondence: xulueqin@163.com

Abstract: Small-to-medium-span girder bridges equipped with shear keys play a significant role in the Chinese highway bridge system. However, shear key failure was observed during the 2008 Wenchuan earthquake, which resulted in excessive superstructure displacements and even catastrophic span collapse. For this, six refined bridges were investigated for the quasi-isolated behaviors under different shear key strengths by using the Pushover and IDA methods. Results indicate that the bridges exhibit two distinct damage states upon the shear key strengths. The shear key failure and bearing sliding create a natural quasi-isolated mechanism, with the following damage sequence: shear key failure → bearing sliding → pier undamaged or slight damage. Quasi-isolated behavior leads to higher displacement demands for beams, especially when the peak ground acceleration (PGA) exceeds 0.45 g. By selecting suitable shear key strength, below 9% for 20 m piers and 30% for 10 m piers, quasi-isolated damage is expected to occur in bridges. The study offers a fresh perspective on the concept of seismic design for highway girder bridges in China.

Keywords: small-to-medium-span girder bridges; shear key; pushover analysis; incremental dynamic analysis (IDA); quasi-isolated behavior

1. Introduction

Small-to-medium-span girder bridges are the mainstay of China's highway bridges, many of which traverse high-intensity earthquake zones. The superstructures of these bridges are simply supported on piers or abutments by unanchored rubber bearings. To restrict the lateral displacement of the girder, reinforced concrete shear keys are installed on both sides of the cap beam and abutment. According to the Chinese seismic design code [1], girder bridges are designed to be ductile, utilizing predesignated plastic hinges in piers to withstand seismic forces. In the 2008 Wenchuan earthquake, a lateral seismic damage survey conducted on 1432 small-to-medium-span girder bridges revealed that, 16.6% of the total bearings suffered severe damage and 19.5% of the total bridge spans experienced lateral movement, including 10 spans that fell off from the supports. Interestingly, the damage proportion of piers was lower than anticipated [2,3]. Furthermore, damage to shear keys was also evidenced in the 1978 Tangshan earthquake [4], the 1994 Northridge earthquake [5], the 1999 Chi-Chi earthquake [6], and the 2010 Chile earthquake [7], revealing similar failure patterns of bridges compared with that in Wenchuan earthquake. The failure of shear keys resulted in the girder losing restraint, ultimately isolating the piers [3]. The isolated failure pattern contradicts the initial intent of the ductile design, highlighting the disparity between China's current seismic concept and engineering practices.

When it comes to the concrete shear keys, there has been a controversial issue associated with their role in the seismic behavior of bridges. While the role of the shear key in bridges has not been well-defined. In China, shear keys are classified as either a structural

measure or secondary component, usually simplified and that disregard the constraining effect or assume the shear key to be rigid body [8,9]. Some codes, such as Caltrans [10], Goe [11] and Savelson [12], also tacitly accept these simplifications. After the Wenchuan earthquake, scholars have since realized that the shear key not only limits displacement but also plays a role in force transmission with digital models of bridges [13,14]. Various types shear keys have been proposed, including the double-layer seismic shear key [15], the sacrifice shear key [16,17], the resettable shear key [18], the wedge shear key [19], the shearing energy dissipation shear key [20], and the X-shaped steel plate shear key [21]. Bi and Hao [22] developed a detailed 3-dimensional finite element model to capture the shear key responses. The results indicated that neglecting the engagement of shear keys might lead to an inaccurate prediction of bridge seismic demands. Están et al. [23] evaluated the influence of external sacrificial shear keys on the seismic behavior of Chilean highway bridges, which concluded that the most vulnerable bridges were those without external shear keys, regardless of the seismic hazards and soil types. These studies concluded that the role of shear keys should not be overlooked. However, the strength of shear keys is frequently either excessive or insufficient due to lack of a design method for shear keys in the Chinese code, leading to significant uncertainties in the seismic response of bridges.

Additionally, the sliding of the superstructure on the unanchored bearing after the shear key failure has also attracted attention, since the sliding acts as isolation [24,25]. Tobias [26] proposed a so-called quasi-isolated bridge system to improve the Illinois Earthquake Resistant System (ERS). The AASHTO [27] stated that the sacrifice of connecting members could effectively weaken the superstructure–substructure connections, thereby limiting seismic forces transferred down to substructures and foundations. The IDOT [28] believed that the essence of the quasi-isolated mechanism lay in achieving a specific fusing mechanism at the connection members between the superstructure–substructure structures, which involved bearing sliding and shear key failure. Filipov [29,30] conducted experimental research on three types of US bearings, and found that bearing sliding results in higher residual displacement. Steelman [31] reached a similar conclusion by utilizing polytetrafluoroethylene bearings to achieve a more reliable quasi-isolated mechanism. Luo [32,33] discovered that achieving quasi-isolated behavior came at the expense of bearing sliding or even beam falling. Wang [34] and Li [35] noted for the study of girder bridges in China that the shear key should be designed as a sacrificial member to achieve the isolation. Nonetheless, there is still a lack of research on the coordination between bearing sliding and beam falling for typical small-to-medium-span girder bridges and are regarded as crucial research needs for further refining quasi-isolated bridge design methodology.

This paper investigated the role of shear keys on the quasi-isolated behavior in typical small-to-medium-span highway girder bridges, taking into account the effects of bearing sliding and shear key degradation. Six typical types of highway girder bridges were investigated for the influence of shear key strength on the transverse quasi-isolated behavior using the Pushover and IDA methods. The quasi-isolated behavior was researched as the failure of the shear key and the slippage of the bearing. The findings provide a basis for the establishment of quasi-isolated concepts.

2. Bridge Case Selection and Research Scope

This research primarily targets typical small-to-medium-span girder bridges in China. Skew bridges, curved bridges, and single-column pier bridges are not within the scope of this study. A typical single-span three-lane highway bridge was selected as the prototype basic bridge case. The bridge spans a U-shaped valley, and the superstructure is a 5 m × 25 m prestressed concrete simple T-beam, as shown in Figure 1. Each T-beam is equipped with a plate-type rubber bearing at both ends, with the bearing type being GJZ250 × 300 × 74 mm. The substructure adopts a round double-column pier, with each pier being 10 m and 1.5 m in diameter. The cap beam and the abutment are equipped with reinforced concrete shear keys. The position of the shear key on the gap beam is shown in Figure 1c, with a 20 mm gap between the shear key and T-beam. The T-beam is constructed

using C40, while the pier, cap beam, and shear key are all made of C30. The bridge site features shallow bedrock and favorable geological sound with a rigid foundation.
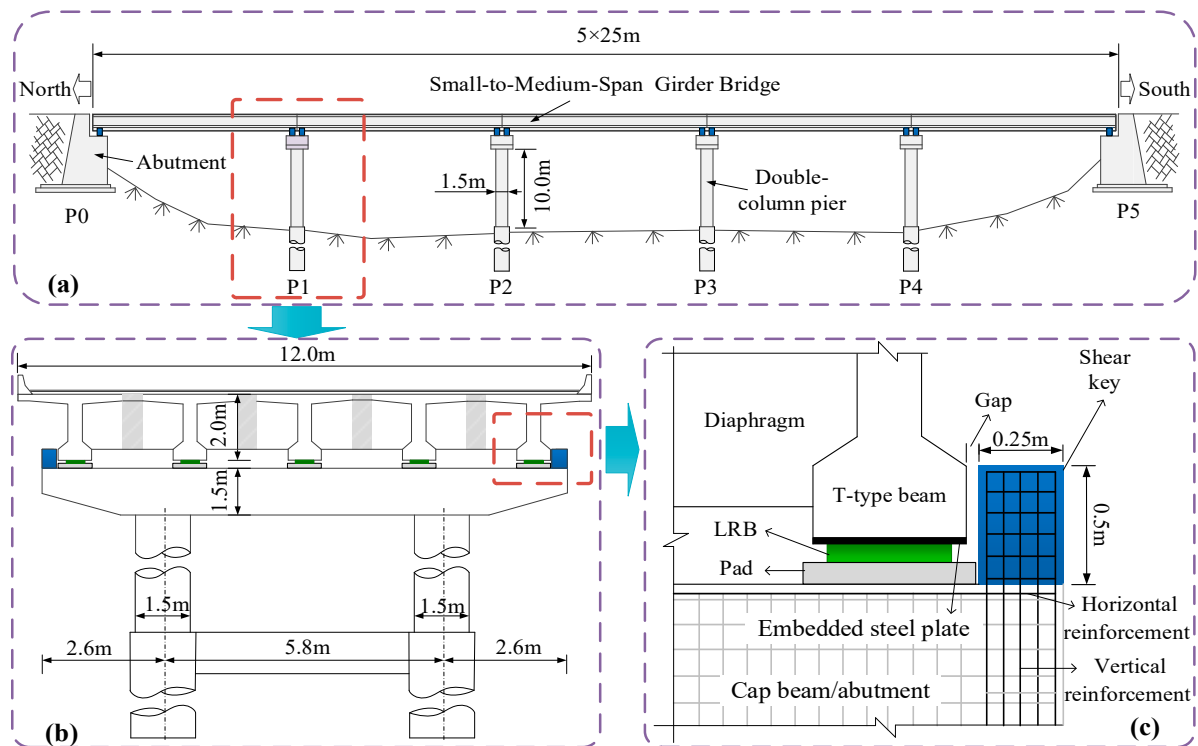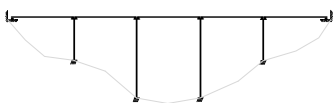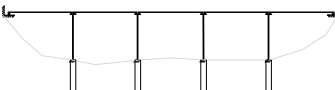

Figure 1. Bridge prototype: (**a**) typical girder bridge; (**b**) cross-sectional diagram; (**c**) shear key installation diagram.

Five other bridge cases are presented to make the research genera; they, are obtained from the above basic bridge case. Parameters include the pier height (10 m or 20 m), span diameter (25 m or 35 m) and foundation form (Rigid or Soft), as shown in Table 1. In addition, the shear key strengths of the different bridge cases were normalized by reference to [36] The shear key strength ratio is defined as the ratio of the shear key strength to the pier or abutment support reaction force, ranging from 0% to 100%. The M10S25Z bridge case introduces a soft soil foundation, which is modeled in the following analysis of pile–soil interaction. The M10S35 signifies that the pier height, pier form, and span of the bridge is 10 m, double-column pier (S), and 35 m, respectively. Table 1 also provides the basic transverse natural vibration period for the M10S35~M10S25Z.

Table 1. Basic information of bridge cases.

Bridge Cases	Pier Forms	Pier Heights	Spans	Foundations	Basic Periods	Illustration Diagrams
M10S25	1.5 m-Double column pier	10 m	5 × 25 m	Rigid	1.09 s	
M10S35	1.5 m-Double column pier	10 m	5 × 35 m	Rigid	1.29 s	
M20S25	1.5 m-Double column pier	20 m	5 × 25 m	Rigid	1.63 s	

Table 1. *Cont.*

Bridge Cases	Pier Forms	Pier Heights	Spans	Foundations	Basic Periods	Illustration Diagrams
M1221S25	1.5 m-Double column pier	10-20-20-10 m	5 × 25 m	Rigid	1.38 s	
M2112S25	1.5 m-Double column pier	20-10-10-20 m	5 × 25 m	Rigid	1.47 s	
M10S25Z	1.5 m-Double column pier	10 m	5 × 25 m	Soft	2.14 s	

3. Model Construction and Verification

3.1. Bearing Sliding Analysis Model

This research primarily targets typical small-to-medium-span girder bridges in China. There is a large amount of literature available for reference on experimental research into the sliding mechanism of the bearing [37,38]. This paper proposes a simplified analysis model based on this, as shown in Figure 2. The bearing undergoes elastic shear deformation before sliding, with the shear stiffness being K_{bH}, and starts to slide when it reaches the critical friction force (F_{bH}). The sliding phenomenon is simulated by the smooth sliding unit in OpenSEES [39], and according to the Coulomb friction theory, the friction coefficient $\mu = 0.25$ is assumed to remain constant during the sliding process. In the formula, G_b is the shear modulus of the rubber, taken as 1200 kN/m^2 according to the regulations [40]; A_b is the area of the bearing rubber plate; t is the total thickness of the rubber layer; and N is the axial force of the bearing. The sliding dynamic constitutive curve of the bearing in the horizontal direction can be calculated, as seen in Figure 2c.

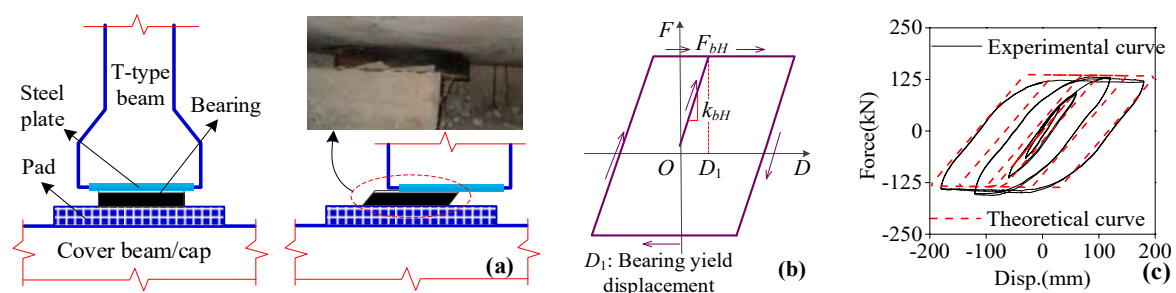$$K_{bH} = G_b A_b / \sum t \tag{1}$$

$$F_{bH} = \mu N \tag{2}$$

Figure 2. Bearing sliding analysis model: (**a**) simplified analysis of bearing sliding damage; (**b**) mechanical model; (**c**) verification analysis.

3.2. Shear Key Mechanical Analysis Model

Earthquake damage [2,3] and experimental research [16,17] show that reinforced concrete shear keys often suffer oblique section shear failure, as shown in Figure 3a,b. The force–deformation curve of the shear key under cyclic load can be decomposed using a two-term nonlinear spring, as shown in Figure 3c. The calculation method of the key node performance parameters corresponding to the two-term spring can be found in the literature [16]. The force–deformation relationship curve of the shear key calculated according to this model fits well with the measured curve, as shown in Figure 3b. There is

generally an installation gap of about 20 mm between the shear key and the main beam in actual engineering, leading to a collision phenomenon between the main beam and the shear key. This paper uses a compression-only gap unit to simulate the shear key, as shown in Figure 3c. It is worth mentioning that the model is also widely adopted, such as Goel [11], Omrani [13], Wu Gang [24], etc.
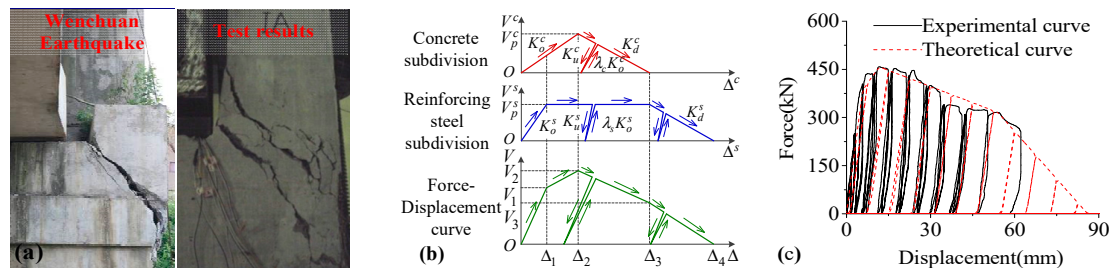

Figure 3. Shear key analysis model: (**a**) comparison of seismic damage and test phenomena; (**b**) simplified analysis; (**c**) verification analysis.

3.3. Pile-Soil Interaction Analysis Model

The pile–column foundation is a foundation form commonly used in the lower structure of girder bridges in China. This paper refers to the pile–soil–bridge pier nonlinear numerical analysis model [41] and establishes a pile–soil analysis model considering silt, clay, and sand soil, as is shown in Figure 4. The pile in the model is simulated by an elastoplastic fiber unit, with a pile length of 20 m, a pile diameter of 1.5 m, and a unit length of 1 m. The pile–soil lateral friction, vertical friction, and pile tip–soil interaction are simulated using the zero-length units of the P-y spring, T-z spring, and Q-z spring in the OpenSEES, respectively. The P-y curve suggested by Matlock is used for clay [42], and the P-y curve suggested by the American API specification is used for sandy soil [43]. The soil-related properties are shown in Figure 4, where φ represents the soil body friction angle; γ represents the soil body bulk density; c_u is the soil body undrained shear strength; ε_{50} represents the strain value when the soil body's 0.5 times the limit principal stress; and C_d represents the ratio of the pile side lateral resistance to the limit soil resistance.
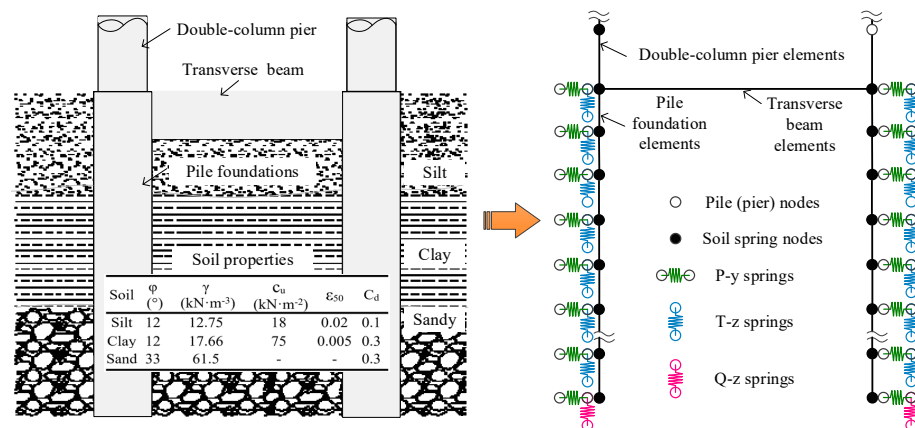

Figure 4. Pile−soil interaction analysis model.

3.4. Whole Bridge Analysis Model

The whole bridge OpenSEES finite element analysis model is shown in Figure 5. The main beam and cap beam are simulated by elastic beam units. The pier column is simulated by elastoplastic fiber units, with concrete and steel bars using the built-in Kent–Scott–Park model and the Giuffré–Menegotto–Pinto model, respectively [39]. The boundary conditions at the abutment are modeled according to the Caltrans simplified method [4]. The prototype bridge case is located in a bedrock, where the nonlinearity of the soil body is

not prominent. To avoid introducing too many complex factors in the analysis, the bridge cases of M10S25~M2112S25 all use rigid foundation modeling, with only the bridge case of M10S25Z considering the pile–soil interaction soft foundation modeling. The whole bridge model is detailed in Figure 5.
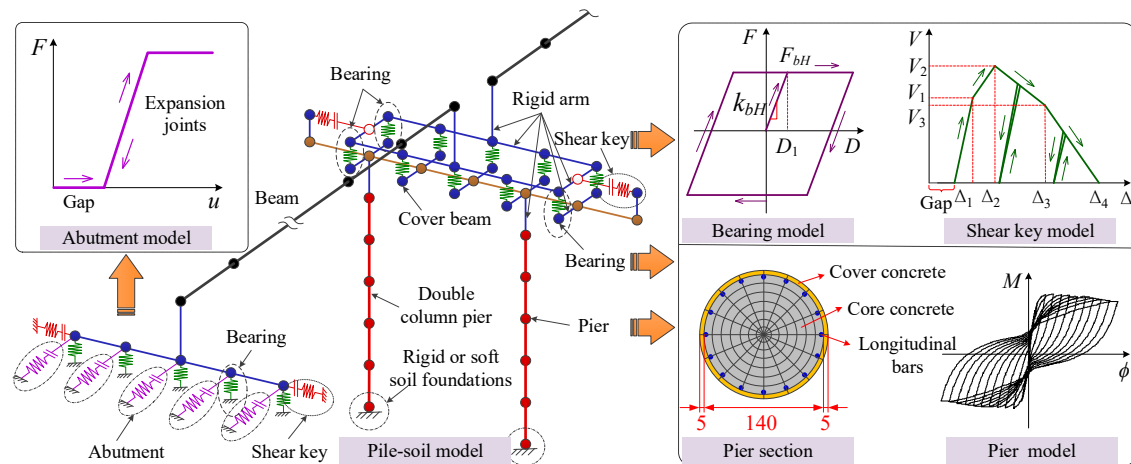

Figure 5. Analytical model of the whole bridge.

4. Analysis Method and Seismic Input

The static elastoplastic analysis method (Pushover method) is used to derive all bridge cases, establishing the damage state derivation curves. The study considers the first-order mode transversely to carry out the derivation analysis, ignoring the contribution of the high-order modes to the structural response [32], with the derivation analysis process shown in the literature [44]. Subsequently, incremental dynamic time history analysis (IDA method) is used for further analysis of the cases. Taking the design response spectrum corresponding to the type II site conditions in the regulations as a benchmark, based on the seismic magnitude M ≥ 6.5, the epicentral distance R ≥ 20 km, and the average shear wave velocity of the 30 m surface soil layer 250 m/s < V_{se} ≤ 500 m/s, 10 seismic waves were selected and amplified from 0.1 g to 1.0 g, as shown in Table 2. The horizontal acceleration response spectrum of the earthquake motion after the PGA = 0.4 g amplification is shown in Figure 6. Among them, T_t represents the first-order natural period of the basic case in the transverse direction. The earthquake motion is only input along the transverse direction, with the average results of the 10 seismic motions taken as its representative value.

Table 2. Ground motion recording parameters.

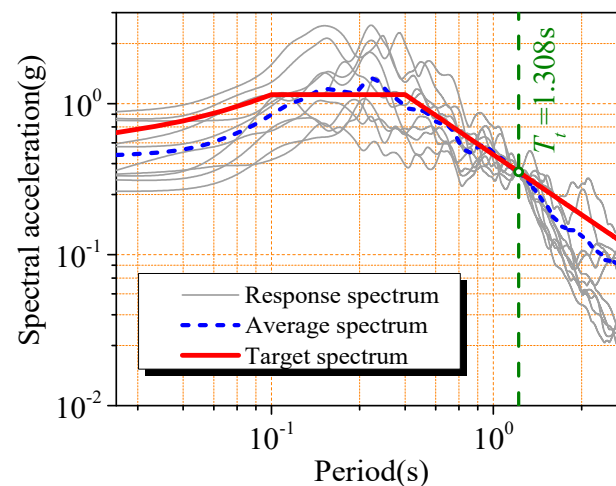| No.	Earthquake Records	Years	Magnitudes	Distance (km)	PGA (g)
1	Wenchuan	2008	8.0	54.5	0.840
2	Imperial Valley	1979	6.5	34.9	0.469
3	Loma Prieta	1989	6.9	76.8	0.103
4	Loma Prieta	1989	6.9	27.3	0.139
5	Landers	1992	7.3	69.2	0.154
6	Landers	1992	7.3	154.3	0.188
7	Northridge	1994	6.7	41.1	0.568
8	Northridge	1994	6.7	57.3	0.432
9	Chi-Chi	1999	7.6	24.9	0.468
10	Chi-Chi	1999	7.6	40.4	0.431

Figure 6. Scaling method of ground motions.

5. Definition of Critical States

5.1. Components Critical States

Components closely related to the quasi-isolated behavior include bearings, shear keys, and bridge piers or abutments. Given that the stiffness and strength of gravity abutments are generally large, the abutments are ignored. The pushover method is used to establish the force–displacement curve of the piers, including 10 m piers under rigid foundation($d_{10m,rigid}$), 20 m piers under rigid foundation($d_{20m,rigid}$) and 10 m piers under soft foundation($d_{10m,soft}$). According to the literature [45], the performance characteristic points corresponding to the first longitudinal reinforcement yielding, cover concrete crushing, core concrete crushing and equivalent yielding are determined. The equivalent bilinearization curve is carried out using the equal energy principle, obtaining the critical yielding displacement (d_y) and critical damage displacement (d_u), as shown in the outer and inner brackets of Figure 7.
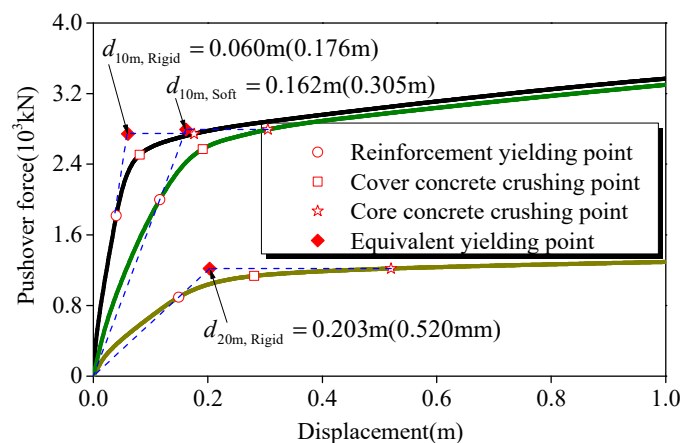

Figure 7. Definition of the pier critical states.

The critical states of the bearing are defined based on existing research results [21]. For the bearing, these are the critical sliding (D_d) and the critical unseating (D_u). The former is equal to the elastic shear deformation (D_1) in Figure 8, which can be calculated by the formulas (1) and (2). The latter is equal to the distance (d_0) plus elastic shear deformation (D_1), in which the distance (d_0) is the maximum distance the support can slip before unseating. The critical values are taken as shown in Table 3.
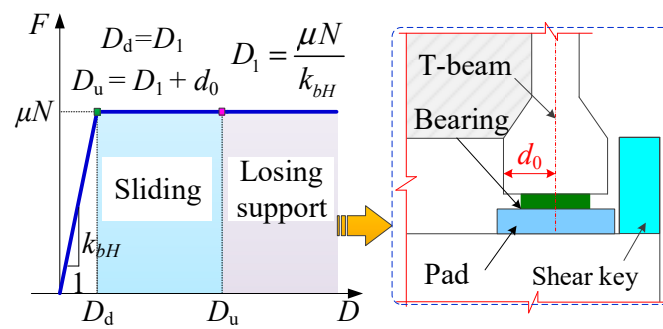
Figure 8. Definition of the bearing critical states.

Table 3. Definition of critical states.

Critical Points	Shear Key (m)	Bearing (m)	Pier (m)		
			$d_{10m,rigid}$	$d_{10m,soft}$	$d_{20m,rigid}$
A	Elasticity (RE)	0.02 (Gap)			
B	0.05 (Δ_d)	Elasticity (SE)			
C	Degradation (RD)	0.053 (D_d)	Elasticity (PE)	Elasticity (PE)	Elasticity (PE)
D	0.158 (Δ_u)	Sliding (SS)			
E		0.353 (D_u)			
F	Damage (RQ)	Losing support (SR)	0.060 (d_y)	0.162 (d_y)	0.203 (d_y)
			Yielding (PF)	Yielding (PF)	Yielding (PF)
G			0.176 (d_u)	0.305 (d_u)	0.520 (d_u)
			Damage (PG)	Damage (PG)	Damage (PG)

The damage critical states of shear keys have been categorized into intensive and degradation phases based on mechanical models [21] in Figure 3. The critical intensive degradation (Δ_d) and critical degradation (Δ_u) are defined in Figure 9. The intensive (Δ_d) and degradation phase (Δ_u) refer to the process of increasing and decreasing resistance provided by the shear key, respectively. Subsequently, the shear key is completely damaged, and fails to restrain the superstructures. The critical values are taken as shown in Table 3.
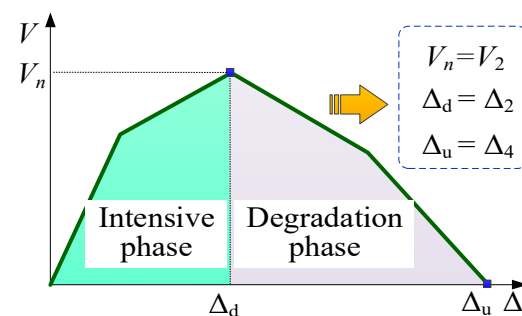

Figure 9. Definition of the shear key critical states.

5.2. System Critical States

Two typical structure systems are established under different shear key strengths by pushover analysis in Figure 10, including the quasi-isolated structural system (QS) and the ductile system (DS). The two systems are based on the relationship of pushover force (i.e., pier foundation force) and displacement. Combining the critical state indicators of each component given in the previous sections, the system critical state of the quasi-isolated

structural system (QS) is divided into five critical points, namely: A~E. The damage state of the quasi-isolated system structure is divided into five states (RE, SE, RD, RQ/SS, SR). In addition, the ductile system (DS) that undergoes ductile failure is divided into two key critical points: F~G. The damaged state of the ductile system (DS) is divided into three states (PE, PF, PG). The definitions of A~G and RE~PG are shown in Figure 10 and Table 3. Table 3 lists the systems and components critical states, and provides judgment criteria and critical values. These critical states will be represented by the initial letter abbreviations shown in the following text.
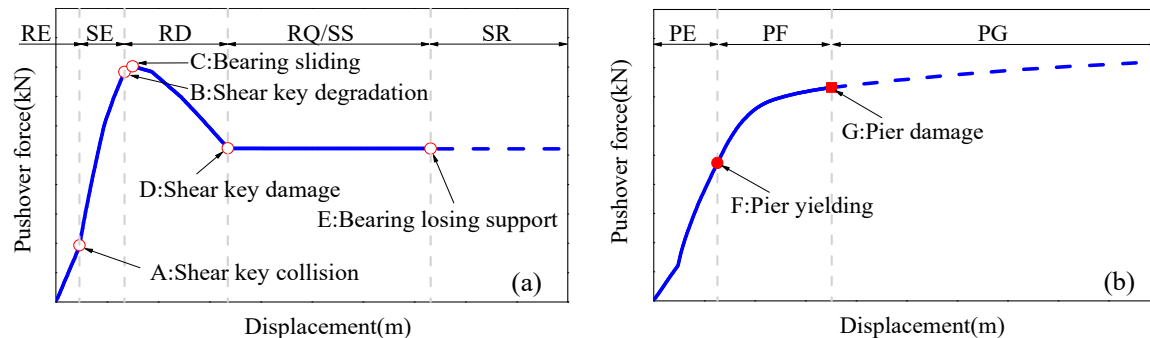

Figure 10. System critical states: (**a**) quasi-isolated system; (**b**) ductility system.

6. Pushover Results

6.1. Quasi-Isolated Behavior of M10S25

Six bridge cases were examined across a range of shear key strengths, varying from 0% to 100%. This ratio signifies the shear key's potency relative to the total supporting reaction force on one side of the pier or abutment. To elucidate, Figure 11 illustrates the system and component responses for M10S25 at shear key strengths of 20% and 60%. At 20%, the shear key strength equates to 0.2 times the support reaction force (2094 kN), approximately 418 kN, and at 60%, it stands at 1254 kN. A0# abutment, 1# pier, and 2# pier are selected for illustration, taking advantage of the symmetry. The pushover curves exhibit distinct trends due to the different shear key strengths. For shear key strengths below 20%, the pushover force (base resistance force) initially increases and subsequently decreases rapidly, reaching a relatively stable range. During this process, the shear keys, bearings, and bridge piers at the A0# abutment and 1# pier maintain an elastic state (B). At 2# pier, the superstructure collides with the shear key (A, B), resulting in bearing slippage (C) and rapid degradation of the shear key (D). After the failure of the shear key (D), bearing friction takes over as the only force transfer mechanism between the superstructure and piers, and the total pier resistance drastically drops. As the displacement keeps increasing, sliding of the bearings initiates (E) and the force transferred to the pier is capped by the kinematic friction. As the lateral force transfer path from the superstructure down to the pier is cut off by shear key failure, resulting in a rapid decrease in base resistance drops substantially. Shear key damage and bearing slipping effectively mitigate the damage to the structural system. This process exemplifies a typical quasi-isolated behavior. Conversely, with shear key strengths surpassing 60%, base resistance force rises proportionally with displacement. In this setup, the shear key exerts robust control over the superstructure, maintaining the bearings in an elastic state. This concurs with the ductile design of bearings as safeguarded components. At 1# pier, elasticity prevails, yielding a notably larger base force than in the quasi-isolated system; yielding (F) and damage (G) manifest at 2# pier. The bridge system then transgresses into a state of severe impairment (PF, PF). This sequence exemplifies a typical ductile behavior. Clearly, an excessive shear key strength renders bridges susceptible to untimely damage and even destruction.
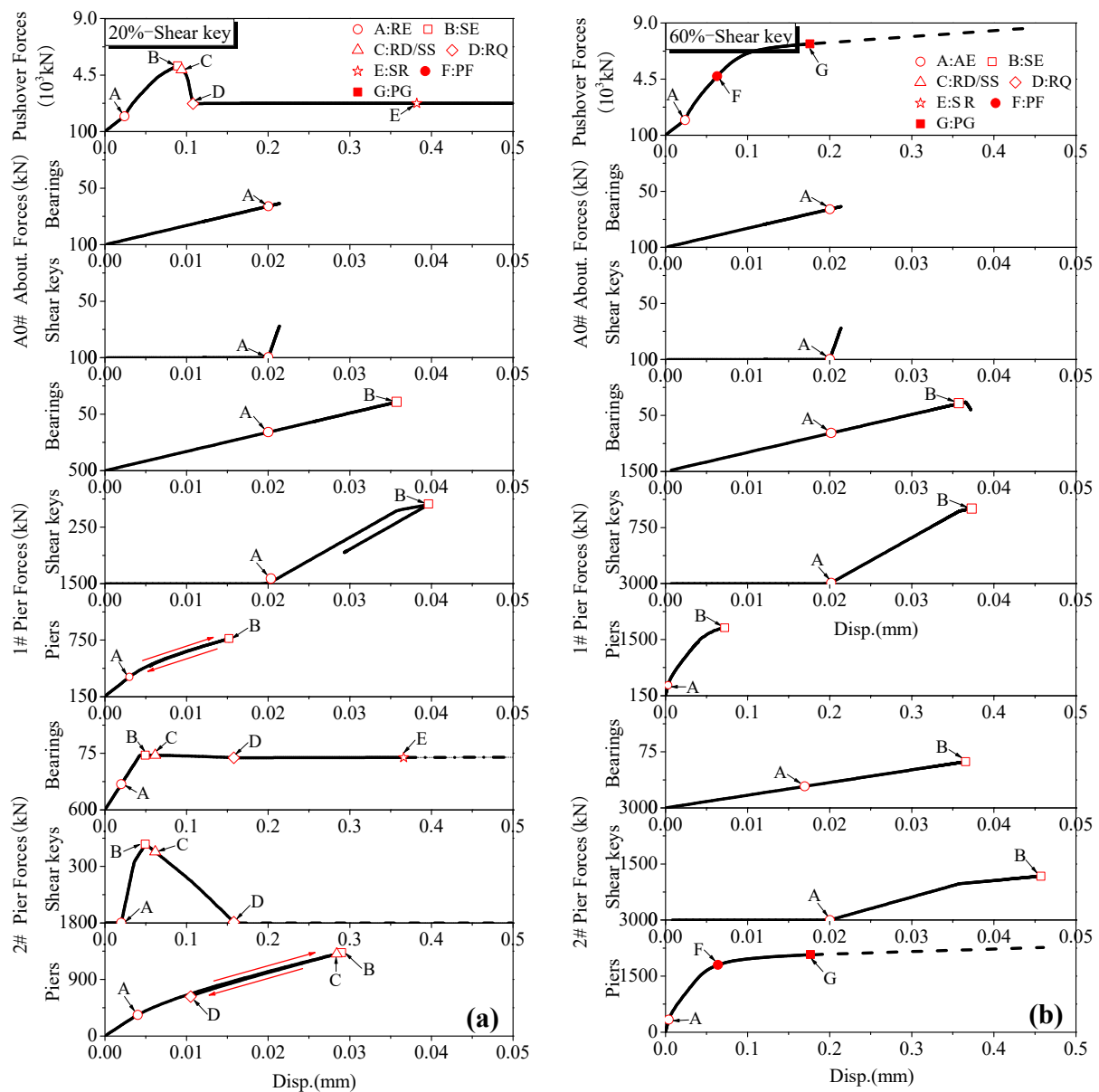
Figure 11. Quasi-isolated behavior of M10S25: (**a**) at 20%; (**b**) at 60%.

6.2. Quasi-Isolated Behavior of M1221S25

Figure 12 illustrates the quasi-isolated behavior curves of M1221S25 across different shear key strengths. Evidently, the pushover curves of M1221S25 exhibit a trend similar to M10S25, with alterations in both component and system behaviors as shear key strengths increase. At low shear key strengths (below 9%), a quasi-isolated behavior prevails. Here, the shear key fractures (b), the bearing slips (c), and the pier remains undamaged (d), leading to a sudden decline in the system's resistance (a). Conversely, when shear key strengths exceed 50%, the shear key and bearing primarily maintain an elastic state, while the pier experiences rapid damage (d), indicating ductile damage. Notably, in comparison to M10S25, M1221S25 demonstrates quasi-isolated behavior with a shear key strength ranging from 3% to 9%.

6.3. Quasi-Isolated Behavior of Other Cases

Figure 13 illustrates the system pushover curves of M10S35, M20S25, M20S25, and M10S25Z. The internal forces and the suitable range of shear key strengths for each bridge case are provided in Table 4. Notably, selecting the appropriate shear key strength can lead

to a reduction of up to 70% in base shear forces. Quasi-seismic behavior can be achieved across all bridge cases, although the required shear key strength varies. For bridges with a 10 m pier, a shear key strength below 30% is effective, while those with a 20 m pier necessitate a relatively smaller shear key strength, specifically below 9%, to realize quasi-isolated behavior. In summary, the strategic selection of shear key strengths can facilitate a shift in bridge damage modes from ductile to quasi-isolated.
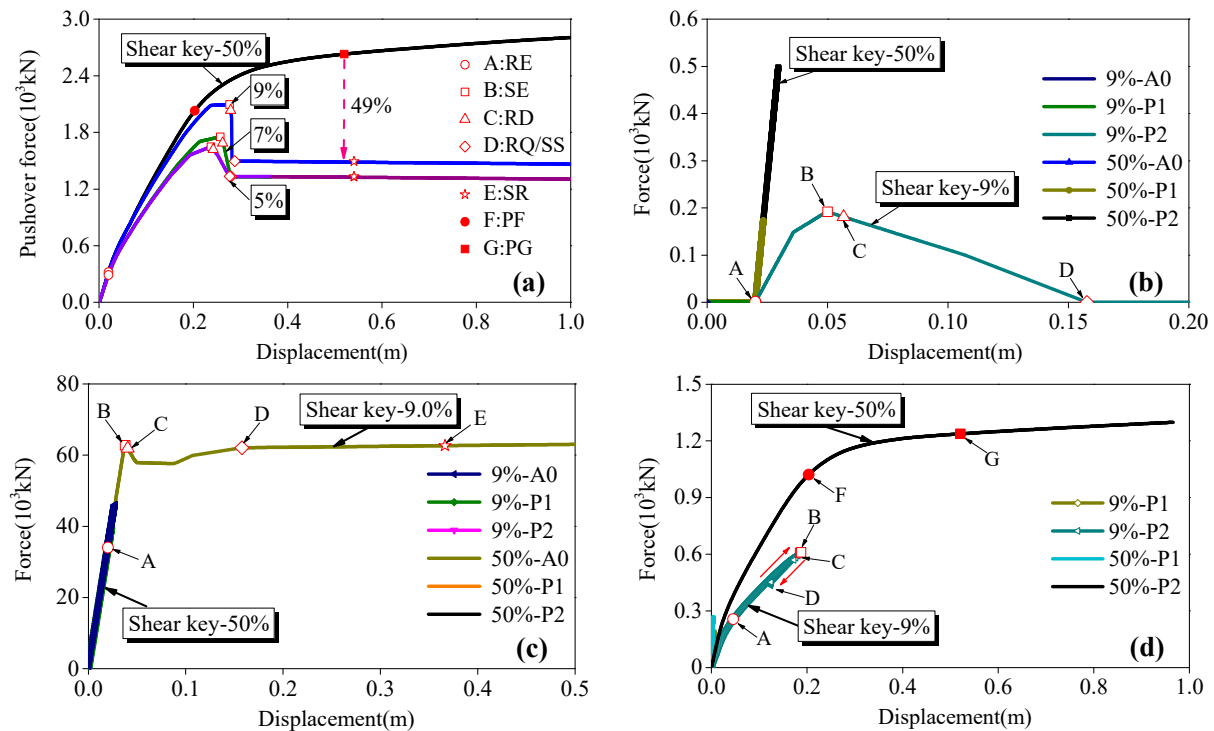
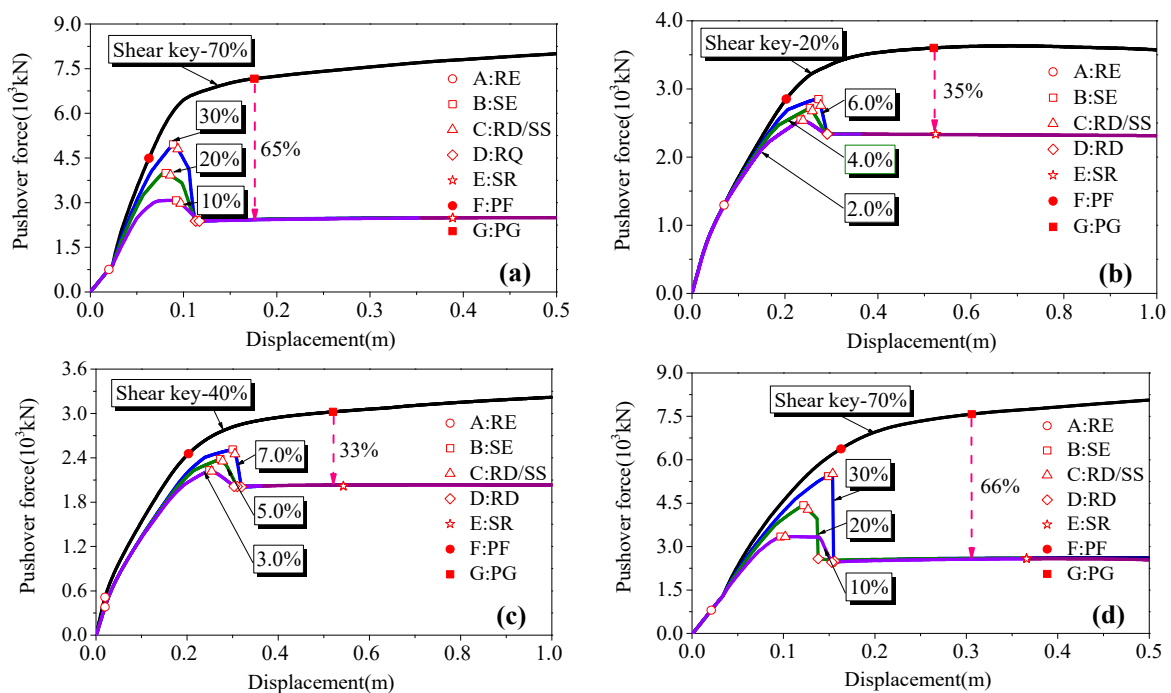**Figure 12.** Quasi-isolated behavior of M1221S25: (**a**) system; (**b**) shear key; (**c**) bearing; (**d**) pier.

Figure 13. Quasi-isolated behaviors of: (**a**) M10S35; (**b**) M20S25; (**c**) M2112S25; (**d**) M10S25Z.

Table 4. Statistics under different shear key strengths of each bridge.

Bridge Cases	Shear Key Strength (%)		Base Shear Force (kN)			Pier Shear Force (kN)			Bearing Disp. (m)	
	DS	QS	DS	QS	Rates	DS	QS	Rates	DS	QS
M10S25	≥60%	10~30%	7320.6	2205.3	70%	2075.4	627.1	70%	0.0366	0.035
M10S35	≥70%	10~30%	7164.9	2482.0	65%	2075.5	800.1	61%	0.0366	0.049
M20S25	≥20%	2~6%	3601.3	2336.6	35%	1114.2	665.7	40%	0.0374	0.366
M2112S25	≥40%	3~7%	3021.6	2019.8	33%	1340.4	740.3	45%	0.0043	0.366
M1221S25	≥50%	5~9%	2630.3	1332.0	49%	1298.8	617.7	52%	0.0295	0.366
M10S25Z	≥70%	10~30%	7578.9	2580.9	66%	1833.3	802.3	56%	0.0256	0.055

7. IDA Results

7.1. Component Time–History Response

Figure 14 depicts the temporal evolution curves of bearing displacement, beam acceleration, and pier displacement for M10S25 under PGA = 0.1 g and PGA = 0.6 g. At lower PGA levels, the seismic responses show minimal discrepancies. In contrast, under higher PGA levels, the peak bearing displacement under 20% shear key strength reaches 0.479 m, which significantly surpasses the value under 60% strength. Concerning the beam acceleration response, a lower shear key strength can effectively limit the peak acceleration reaction of the beam, regardless of the PGA magnitude. Under increased PGA levels, the pier subjected to 20% shear key strength is approaching yielding, whereas the pier with 60% strength has already sustained substantial damage. A more robust shear key exerts a more adverse influence on the seismic behavior of the substructure, especially under high PGA conditions. Excessive shear key strength can lead to premature damage of the bridge.

7.2. Component Damage States

Figures 15–20 present the damage states of components for the 2# pier in each case, considering both lower and higher shear key strengths. The critical accelerations at which components transition to distinct states are indicated in parentheses. Overall, with an increase in PGA, components progressively enter distinct damage states, revealing diverse sequences of component damage. In the case of M10S25, under shear key strengths of 20% and 60%, the former remains undamaged, whereas the latter has already yielded at accelerations of 0.282 g and undergone significant damage at 0.65 g. Under 60% shear key strength, the pier experiences the initial component damage, while under 20% shear key strength, bearing slippage triggers an isolation phenomenon, deferring the damage onset and reducing the extent of damage. A similar quasi-isolated phenomenon can also be observed in other cases of M10S35~M10S25Z. The piers of these bridges exhibit yielding under two shear key strengths. In M10S35, the damage onset of the pier occurs earlier at 70% than at 20%, with accelerations of 0.228 g and 0.721 g, respectively. Moreover, the damage extent at 70% is also more severe than at 20%, resulting in significant damage to the piers. In summary, lower shear key strengths delay the damage and reduce the extent of damage, representing acceptable quasi-isolated behavior.

7.3. System Damage States

Figure 21 illustrates the damage state curves for each bridge system, established using the total pier base shear forces. The minimum acceleration at which all components transition to the critical state is indicated within parentheses. Furthermore, the figure depicts the rate of change of basal shear force at the point (G) of severe damage. The alteration in the system's base shear force is significant, with a maximum reduction of 37.3%. This alteration is observed in the figure to occur subsequent to the damage (D) of the shear key. In terms of the system's damage states, with higher shear key strength,

predominant damage occurs on the piers (F, G), while the shear key and bearing remain intact. Conversely, when shear key strength is low, the shear key is more susceptible to damage, followed by the bearing and then the pier. However, the order in which damage occurs does not strictly adhere to a specific pattern. Notably, the piers of M10S25 consistently remained undamaged. In the cases of M20S25, M2112S25, and M10S25Z, the piers yielded earlier than the bearing, albeit generally with minor damage.
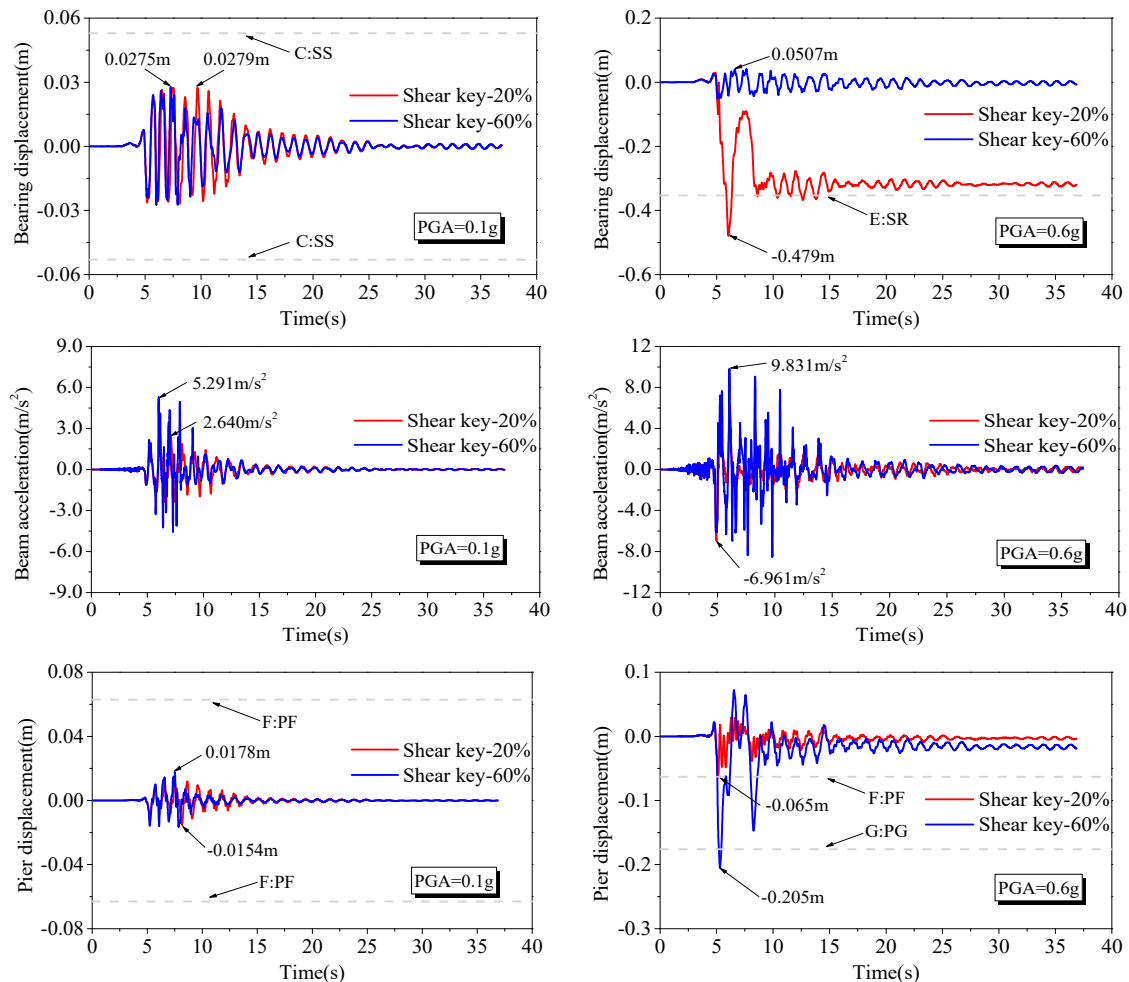
Figure 14. Time-history curves of M10S25 under PGA = 0.1 g and PGA = 0.6 g.
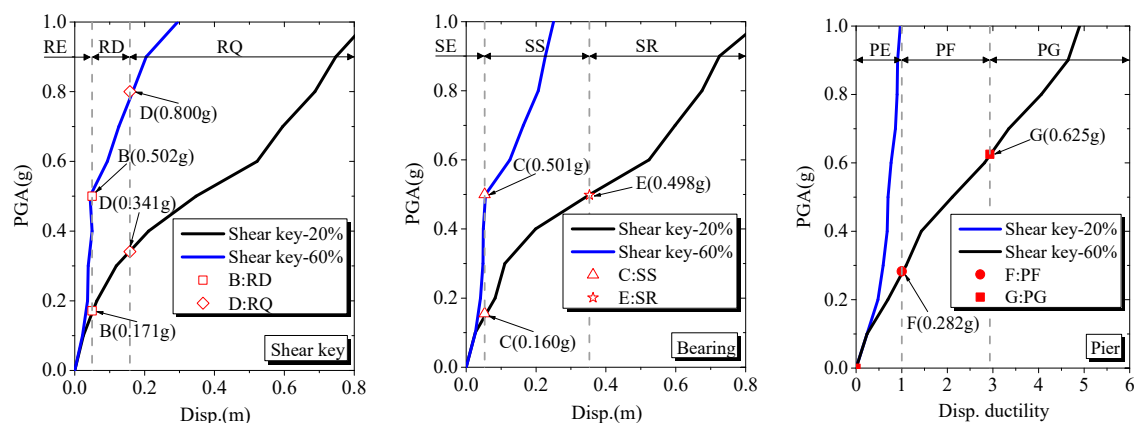
Figure 15. Components damage states of M10S25.
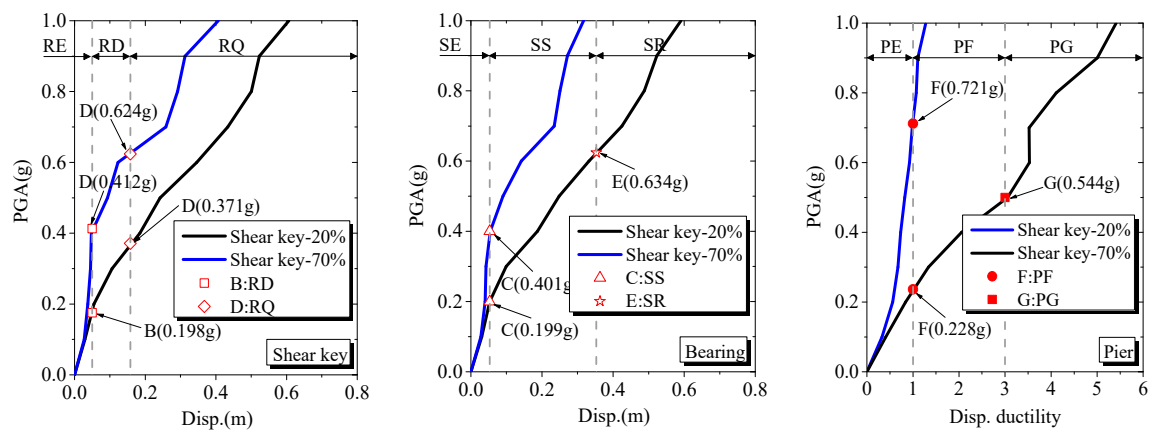
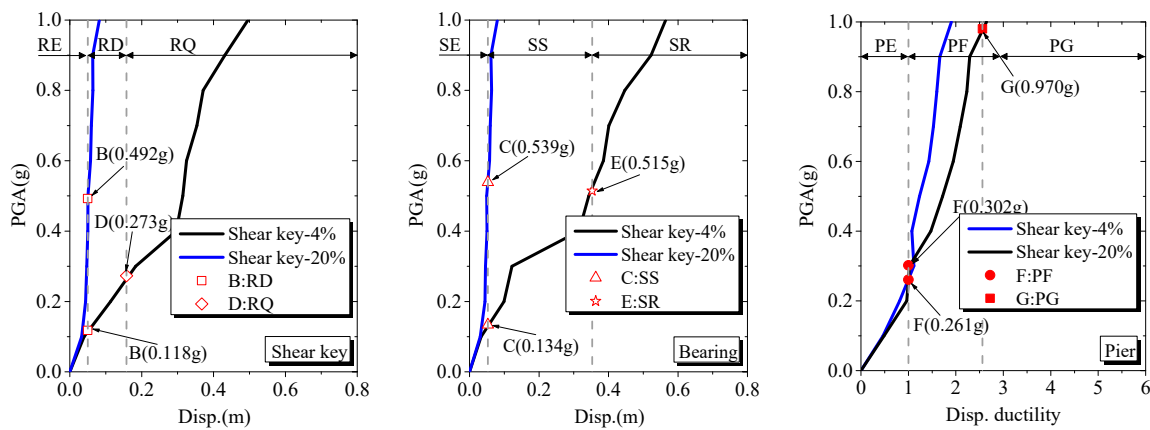**Figure 16.** Components damage states of M10S35.

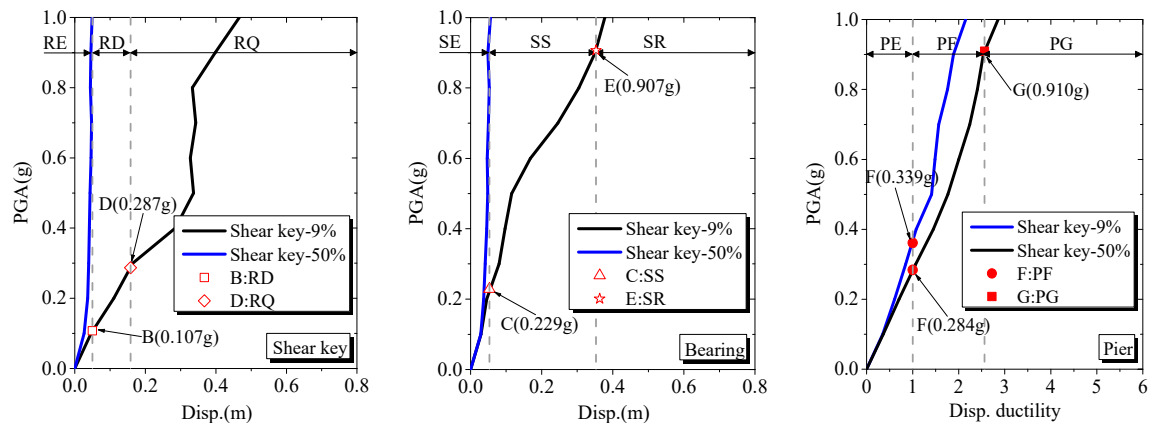**Figure 17.** Components damage states of M20S25.

Figure 18. Components damage states of M1221S25.

7.4. Beam Displacement Demands

Figure 22 shows the displacement demand of the main beam, which is represented by the peak displacements of the bearings at different PGAs. Differentiating among colors, green, yellow, and orange correspond to the bearing states of elasticity, slip (0.053 m), and unseating (0.353 m) correspondingly. Darker shades indicate an escalated potential for bearing unseating. The demand for bearing displacement increases with reduced shear key strength, exceeding that at higher shear key strength, consequently resulting in inevitable bearing slippage. The bearing displacement under lower shear key strength (solid points) consistently surpasses that, signifying a marked residual displacement during quasi-isolated behavior. Notably, there is a risk that the main beam will lose support

under a certain acceleration. The likelihood of bearing unseating is inconsequential when the ground motion probability is below 0.45 g. Nevertheless, within earthquake zones characterized by the PGA of ground motion exceeding 0.45 g, this risk cannot be ignored and a deliberation arises concerning the equilibrium between permitting bearing sliding and averting bearing unseating.
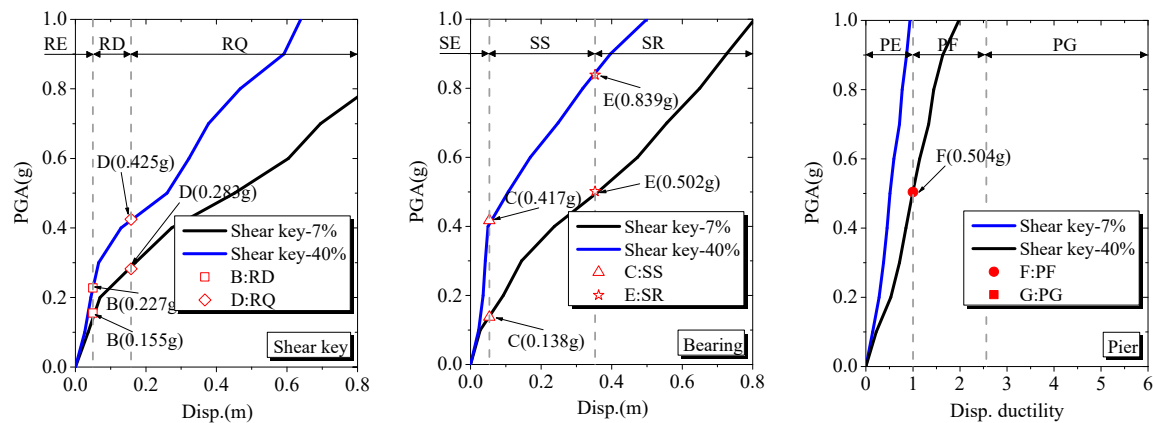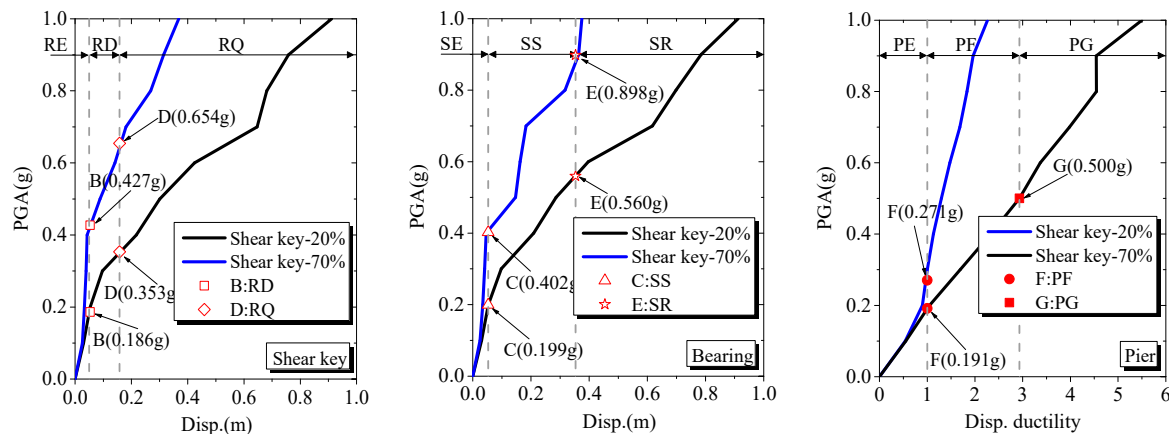
Figure 19. Components damage states of M2112S25.

Figure 20. Components damage states of M10S25Z.

7.5. Damage Sequencs

Figure 23 presents a comparison of the damage sequence for each bridge under the two shear key strengths. The progression of each component through specific damage states is indicated. Let us take M10S25 as an example. At 60% shear key strength: 1PF@1#Pier → 2PF@2#Pier → 3SS@2#Pier → 4SS@A0#Abutment → 5SS@2#Pier → 6PG@2#Pier → 7SR@2#Pier → 8PG@1#Pier → 9SR@A0#Abutment. At 20% shear key strength: 1SS@2#Pier → 2SS@1#Pier → 3SS@A0#Abutment → 4SR@2#Pier → 5SR@1#Pier → 6SR@A0#Abutment. The observation reveals that, at 60% strength, the substructure (PF, PG) is primarily affected initially. In contrast, at 20% strength, the superstructures experience the initial impact, involving shear key failure (SR) and bearing slip (SS), with no significant effect on the piers. This similar damage sequence is observed in other bridge cases, which can be classified into two types: quasi-isolated damage and ductile damage. Quasi-isolated damage sequence: shear key damage → bearing slip → pier undamaged or slight damage. Ductile damage sequence: pier damage → bearing slip → pier serious damage. In summary, the most favorable damage sequence is the one aligned with quasi-isolated behavior, where the bridge undergoes minimal structural impairment.
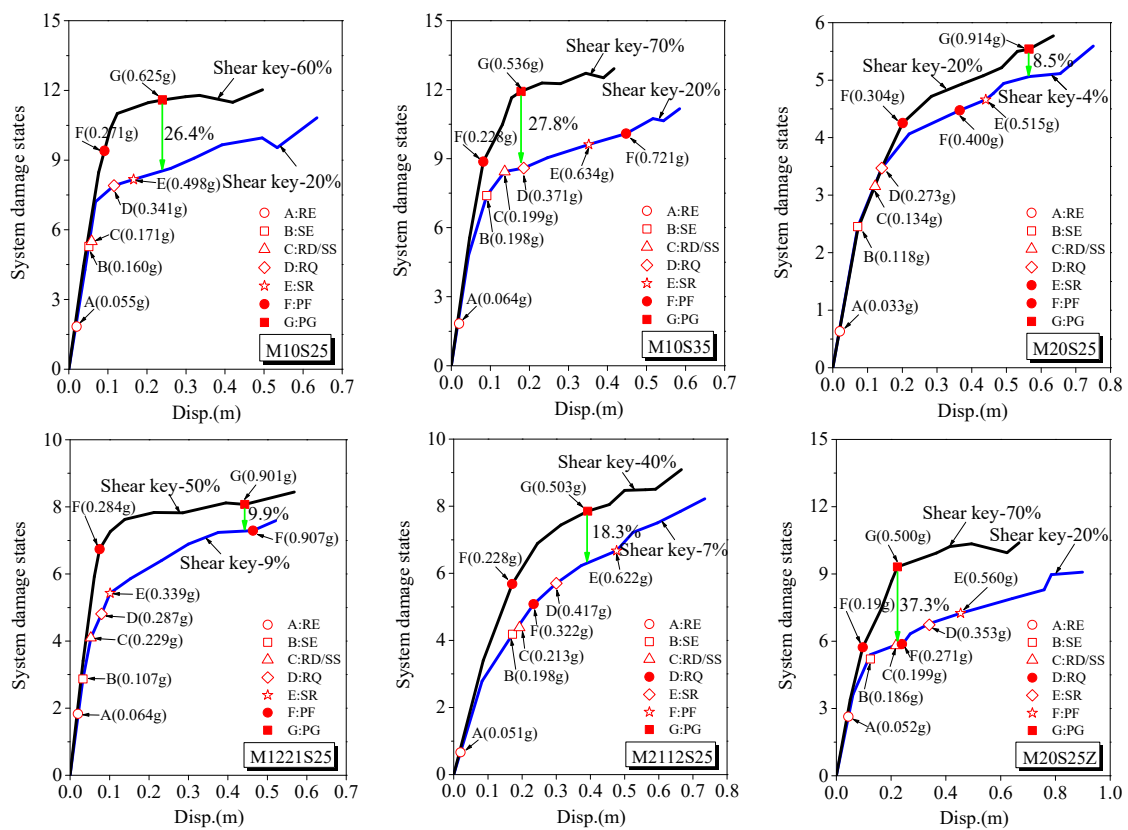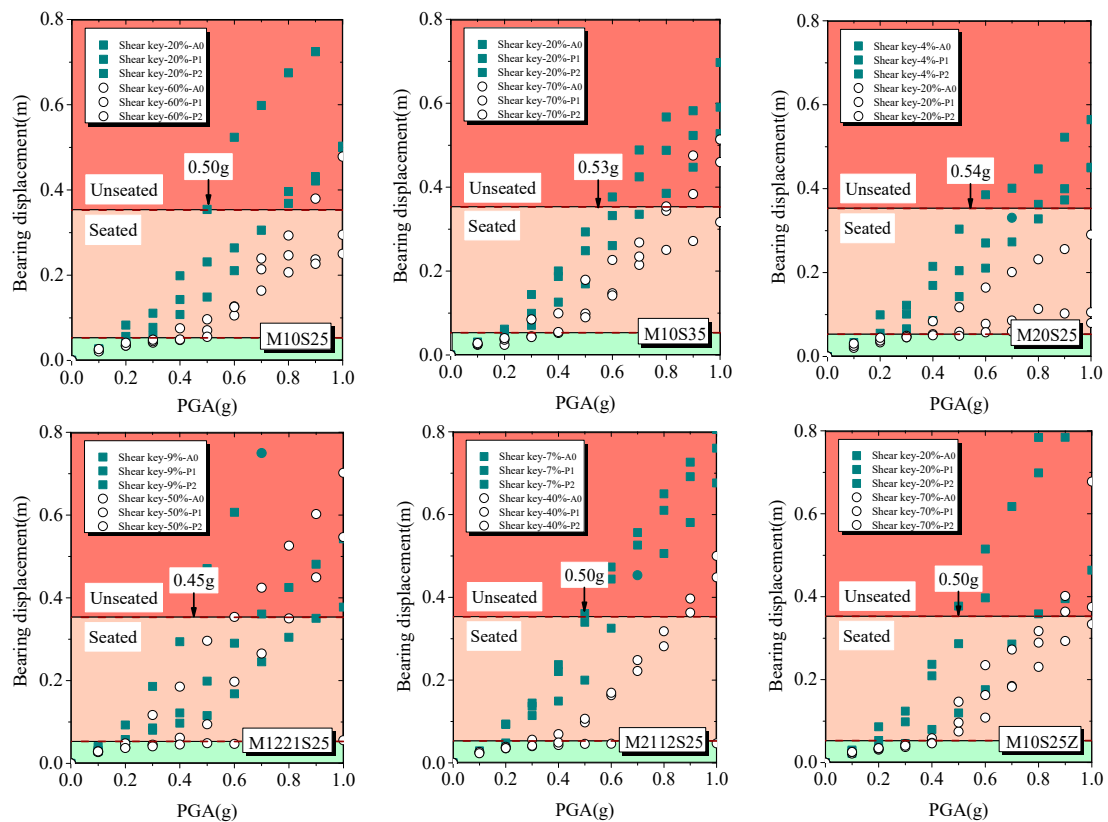
Figure 21. System damage states.

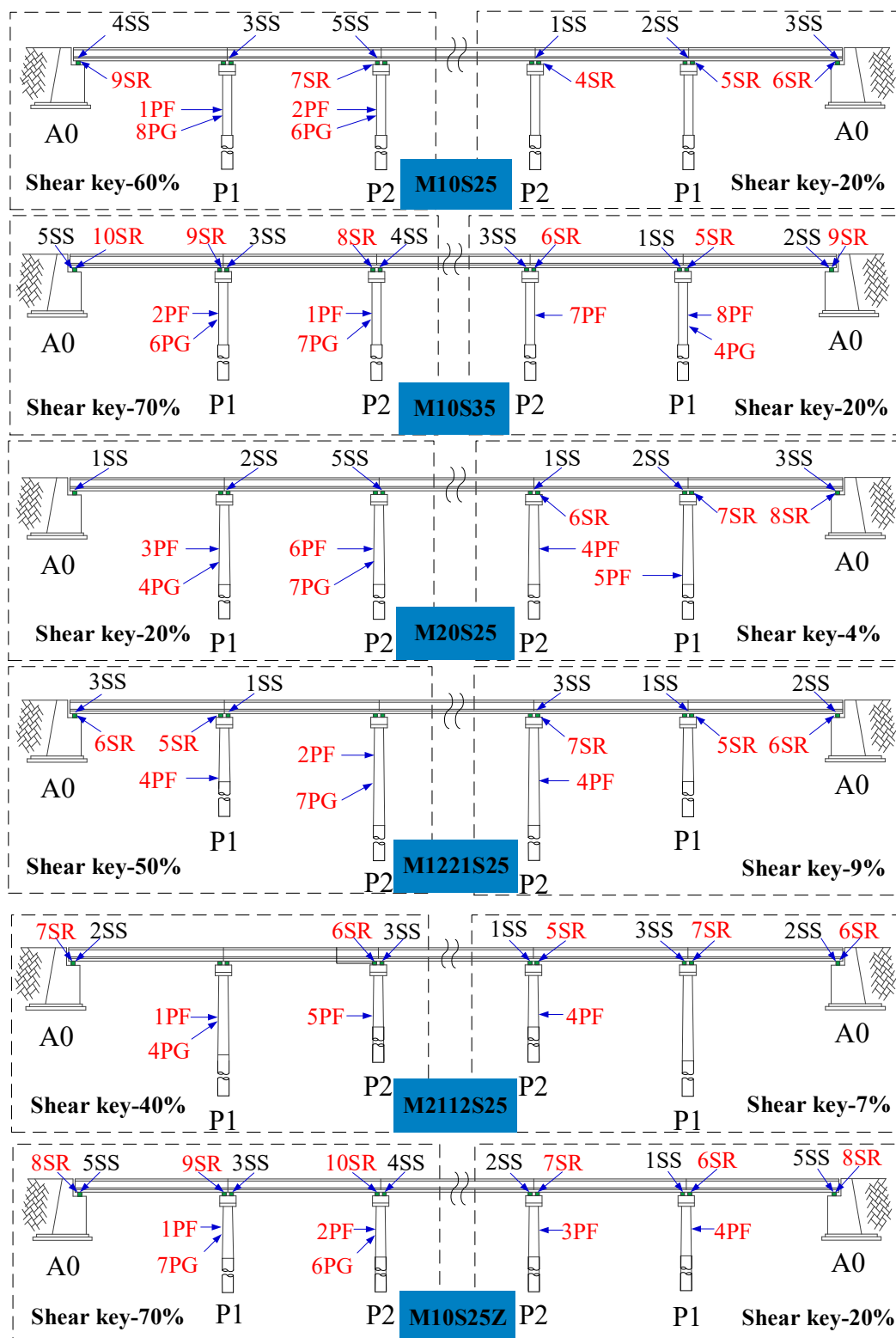**Figure 22.** Beam displacement demands.

Figure 23. Bridge damage sequences.

7.6. Damage Patterns

Figure 24 provides the damage patterns of each bridge case. Notably, when subjected to a larger shear key strength (black line), bridges tend to enter the yellow and orange zones earlier, unlike those with a smaller shear key strength (red line). These observations hold despite the bridges having varying spans, pier heights, combination forms, and foundation

types. Quasi-isolated behavior has been observed across these variations, even though they exhibit distinct damage sequences. The damage sequence of a bridge is not obligated to follow a specific pattern, aligning with the principles of the quasi-isolated strategy. An optimal quasi-isolated damage sequence involves: shear key damage → bearing slip → pier undamaged or slight damage. By opting for a smaller shear key strength, the damage patterns of bridges can transition from ductile failure to quasi-isolated failure, effectively mitigating premature and excessive structural damage.
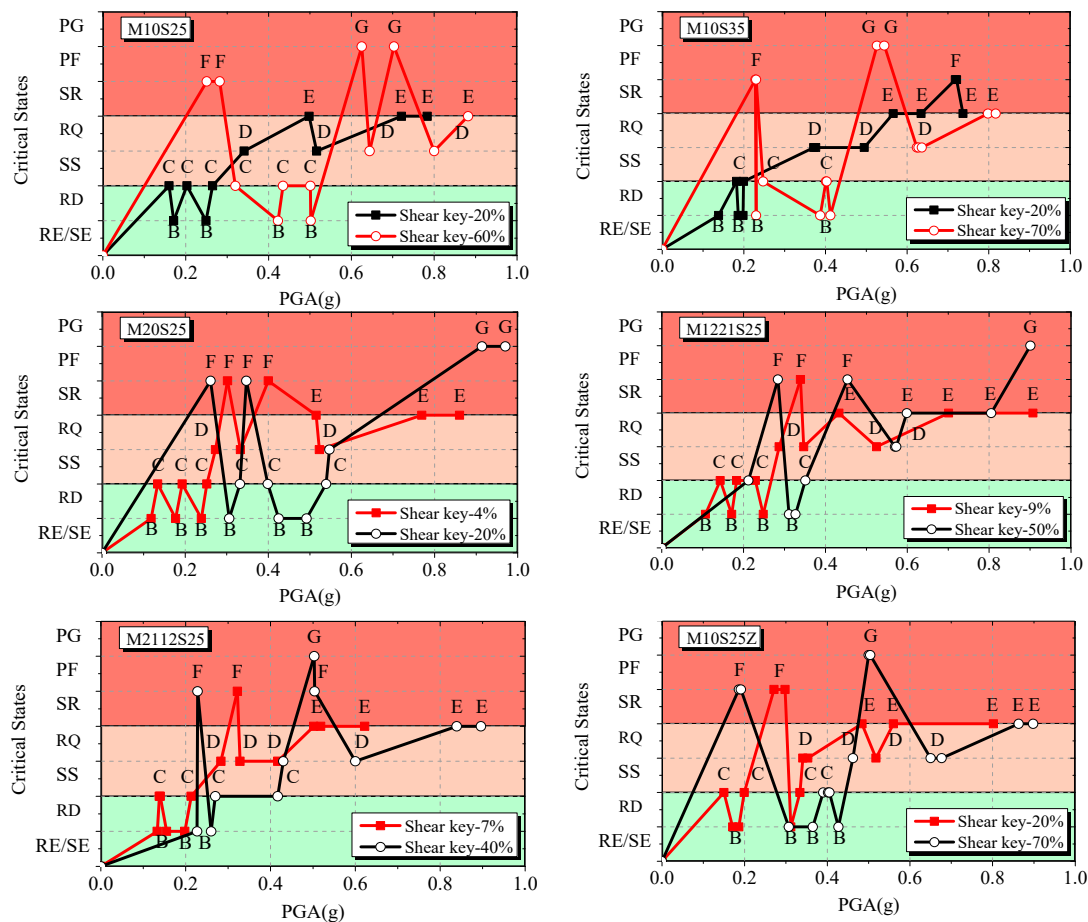

Figure 24. Bridge damage patterns.

8. Conclusions

This study employs the Pushover and the IDA methods to comparatively analyze the influence of shear keys on the quasi-isolated behavior of typical small-to-medium-span girder bridges. The key conclusions are summarized as follows:

(1) The bridge exhibits two distinct damage states upon the shear key strengths. At larger shear key strength, the bridge is damaged quickly. In cases where the shear key strength is lower, the base shear force declines, up to 70%. The bridges remain undamaged or slight damage due to the failure of shear key, which is a typical quasi-isolated behavior.

(2) In quasi-isolated bridges, the superstructure of bridges tends to generate larger displacement demands, which increases the risk of bridge unseating and, potentially, beams falling off. This concern becomes particularly pronounced in seismically active regions where the peak ground acceleration (PGA) exceeds 0.45 g.

(3) The damage sequence can be classified into two types: quasi-isolated damage and ductile damage. The quasi-isolated damage sequence is: shear key failure → bearing

slip → pier undamaged or slight damage. The damage sequence is not required to adhere to any specific pattern, which is permissible under the quasi-isolated strategy.

(4) By selecting suitable shear key, the response of the bridge during seismic events will shift from ductile damage to quasi-isolation damage. Optimal recommendations suggest maintaining the shear key strength ranging from 10% to 30% for bridges with 10 m piers, while for bridges with 20 m piers, a more suitable range lies between 2% and 9%.

(5) For typical highway girder bridges in China, selecting a lower and suitable shear key strength from the above range can effectively prevent premature damage to the bridges. This quasi-isolated strategy, which involves sacrificing auxiliary components to achieve isolated, offers a significant advantage in seismic fortification.

References

1. *JTG/T 2231-01-2020*; Code for Seismic Design of Highway Bridges. China Communications Press: Beijing, China, 2020. (In Chinese)
2. Zhuang, W.L.; Liu, Z.Y.; Jiang, J.S. Analysis and countermeasures for the earthquake damage of highway bridges in Wenchuan, 5.12. *Southwest Highw.* **2009**. (In Chinese)
3. Du, X.L.; Han, Q.; Li, Z.X.; Li, L.Y.; Chen, S.F.; Zhao, J.F. Seismic damage of mountain highway bridges in the 5.12 Wenchuan earthquake and its inspiration. *J. Beijing Univ. Technol.* **2008**, *34*, 1270–1279.
4. Ding, J.; Jiang, S.; Bao, F. Review of bridge damage caused by Tangshan earthquake. *World Seismol. Eng.* **2006**, *22*, 68–71. (In Chinese)
5. Broderick, B.M.; Elnashai, A.S. Analysis of the failure of interstate 10 freeway ramp during the Northridge earthquake of 17 January 1994. *Earthq. Eng. Struct. Dyn.* **1995**, *24*, 189–208. [CrossRef]
6. Lu, C.H.; Liu, K.Y.; Chang, K.C. Seismic performance of bridges with rubber bearings: Lessons learnt from the 1999 Chi-Chi earthquake. *J. Chin. Inst. Eng.* **2011**, *34*, 889–904. [CrossRef]
7. Schanack, F.; Valdebenito, G.; Alvial, J. Seismic damage to bridges during the 27 February 2010 magnitude 8.8 Chile earthquake. *Earthq. Spectra* **2012**, *28*, 301–315. [CrossRef]
8. Nie, L.Y.; Li, J.Z.; Fan, L.C. Selection of pounding analysis parameters and its effects on structure under earthquake. *Eng. Mech.* **2005**, *22*, 142–146. (In Chinese) [CrossRef]
9. Liu, P.; Zheng, K.F.; Yang, L.; Wu, Z.W. Numerical method for bridge seismic response considering beam-shear key pounding effect. *Northwest. Seismol. J.* **2011**, *33*, 336–341. (In Chinese) [CrossRef]
10. SDC. *Caltrans Seismic Design Criteria Version 1.7*; California Department of Transportation: Sacramento, CA, USA, 2013.
11. Goel, R.K.; Chopra, A.K. Role of shear keys in seismic behavior of bridges crossing fault-rupture zones. *J. Bridge Eng.* **2008**, *13*, 398–408. [CrossRef]
12. Salveson, M.W.; Fell, B.V. Effect of abutment shear keys on the seismic response of bridges. In Proceedings of the Structures Congress 2011, Las Vegas, NV, USA, 14–16 April 2011. [CrossRef]
13. Omrani, R.; Mobasher, B.; Sheikhakbari, S. Variability in the predicted seismic performance of a typical seat-type California bridge due to epistemic uncertainties in its abutment backfill and shear-key models. *Eng. Struct.* **2017**, *148*, 718–738. [CrossRef]
14. Nicoletti, V.; Martini, R.; Carbonari, S.; Gara, F. Operational Modal Analysis as a Support for the Development of Digital Twin Models of Bridges. *Infrastructures* **2023**, *8*, 24. [CrossRef]
15. Wang, K.H.; Hui, Y.X.; Wu, G. Study on seismic performance of seismic double-layer stopper. *Earthq. Eng. Eng. Dyn.* **2014**, *34*, 505–510. (In Chinese)
16. Xu, L.Q.; Li, J.Z. Design and experimental investigation of a new type sliding shear key and its efficacy in seismic fortification. *Eng. Mech.* **2016**, *33*, 111–118. (In Chinese) [CrossRef]

17. Xu, L.Q.; Li, J.Z. A two-level design method for sacrificeable seismic blocks. *Chin. J. Highw.* **2015**, *28*, 59–66. (In Chinese)

18. Han, Q.; Zhou, Y.; Ou, Y.; Du, X. Seismic behavior of reinforced concrete sacrificial exterior shear keys of highway bridges. *Eng. Struct.* **2017**, *139*, 59–70. [CrossRef]

19. Zhao, J.; Xiang, C.S.; Zhou, Y.; Liu, G.S. Effect of wedge block on the transverse seismic performance of small-and-medium-span girder bridges. *China Earthq. Eng. J.* **2020**, *42*, 22–31. (In Chinese)

20. Deng, K.; Pan, P.; Su, Y.; Ran, T.; Xue, Y. Development of an energy dissipation restrainer for bridges using a steel shear panel. *J. Constr. Steel Res.* **2014**, *101*, 83–95. [CrossRef]

21. Xiang, N.L.; Alam, M.S.; Li, J. Yielding Steel Dampers as Restraining Devices to Control Seismic Sliding of Laminated Rubber Bearings for Highway Bridges: Analytical and Experimental Study. *J. Bridge Eng.* **2019**, *24*, 04019103.1–04019103.15. [CrossRef]

22. Bi, K.; Hao, H. Modelling of shear keys in bridge structures under seismic loads. *Soil Dyn. Earthq. Eng.* **2015**, *74*, 56–68. [CrossRef]

23. Están, J.J.W.; Santa María, H.; Riddell, R.; Arrate, C. Influence of the use of external shear keys on the seismic behavior of Chilean highway bridges. *Eng. Struct.* **2017**, *147*, 613–624. [CrossRef]

24. Wu, G.; Wang, Q.L.; Wang, K.H.; Zhang, P.P. Transverse seismic response analysis for bridges considering performance degradation of bearings and stoppers. *J. Vib. Shock* **2018**, *37*, 189–196. (In Chinese)

25. Li, Y.; Li, C.; Li, X. Effect of sliding of plate rubber bearings on seismic performance of small and medium span girder bridges under seismic action. *J. Civ. Eng.* **2014**, *47* (S1), 124–129. (In Chinese)

26. Tobias, D.H.; Anderson, R.E.; Hodel, C.E.; Kramer, W.M.; Wahab, R.M.; Chaput, R.J. Overview of earthquake resisting system design and retrofit strategy for bridges in Illinois. *Pract. Period. Struct. Des. Constr.* **2008**, *13*, 147–158. [CrossRef]

27. AASHTO. *AASHTO LRFD Bridge Design Specifications*; American Association of State Highway and Transportation Officials: Washington, DC, USA, 2012.

28. IDOT. *Illinois Department of Transportation. Standard Specification for Road and Bridge Construction*; IDOT: Springfield, IL, USA, 2007.

29. Filipov, E.T.; Fahnestock, L.A.; Steelman, J.S.; Hajjar, J.F.; LaFave, J.M.; Foutch, D.A. Evaluation of quasi-isolated seismic bridge behavior using nonlinear bearing models. *Eng. Struct.* **2013**, *49*, 168–181. [CrossRef]

30. Filipov, E.T.; Revell, J.R.; Hnestock, L.A.; Lafave, J.M.; Hajjar, J.F.; Foutch, D.A. Seismic performance of highway bridges with fusing bearing components for quasi-isolated. *Earthq. Eng. Struct. Dyn.* **2013**, *42*, 1375–1394. [CrossRef]

31. Steelman, J. Sacrificial Bearing Components for Quasi-Isolated Response of Bridges Subject to High-Magnitude, Low-Probability Seismic Hazard. Ph.D. Thesis, University of Illinois at Urbana-Champaign, Urbana, IL, USA, 2013. Available online: https://hdl.handle.net/2142/45455 (accessed on 22 August 2013).

32. Jie, L.; Fahnestock, L.A.; Lafave, J.M. Nonlinear Static Pushover and Eigenvalue Modal Analyses of Quasi-Isolated Highway Bridges with Seat-Type Abutments. *Structures* **2017**, *12*, 145–167. [CrossRef]

33. Luo, J.; Fahnestock, L.A.; Lafave, J.M. Seismic Performance Assessment of Quasi-Isolated Highway Bridges with Seat-Type Abutments. *J. Earthq. Eng.* **2019**, *25*, 2285–2324. [CrossRef]

34. Wang, K.H.; Wei, H.; Li, X.; Li, R. Seismic design concepts for small and medium span highway bridges. *J. Civ. Eng.* **2012**, *45*, 115–121. (In Chinese)

35. Li, J.Z.; Tang, H.; Guan, Z.G. A new isolation system for small and medium span bridges on laminated rubber bearings. *China J. Highw. Transp.* **2015**, *28*, 35–43. (In Chinese)

36. Xiang, N.; Li, J. Effect of exterior concrete shear keys on the seismic performance of laminated rubber bearing-supported highway bridges in China. *Soil Dyn. Earthq. Eng.* **2018**, *112*, 185–197. [CrossRef]

37. Steelman, J.S.; Fahnestock, L.A.; Filipov, E.T. Shear and friction response of nonseismic laminated elastomeric bridge bearings subject to seismic demands. *J. Bridge Eng.* **2013**, *18*, 612–623. [CrossRef]

38. Xiang, N.; Li, J. Experimental and numerical study on seismic sliding mechanism of laminated-rubber bearings. *Eng. Struct.* **2017**, *141*, 159–174. [CrossRef]

39. Mazzoni, S.; McKenna, F.; Scott, M.H. *Open System for Earthquake Engineering Simulation: OpenSees Command Language Manual*; Pacific Earthquake Engineering Center: Berkeley, CA, USA, 2007. [CrossRef]

40. *JT-T 4-2019*; Plate-Type Elastomeric Pad Bearings for Highway Bridges. China Communication Press: Beijing, China, 2019. (In Chinese)

41. Zhang, X.Y.; Tang, L.; Ling, X.C.; Su, L.; Liu, C.H.; Gao, X. Characterization of pile-soil dynamic interaction p-y curves for bridges at liquefaction sites. *J. Disaster Prev. Mitig. Eng.* **2014**, *5*, 619–625. (In Chinese)

42. API Recommended Practice 2A-WSD (RP 2A-WSD). *Recommended Practice for Planning, Designing, and Constructing Fixed Offshore Platforms-Working Stress Design*; American Petroleum Institute: Washington, DC, USA, 2002.

43. Lymon, C. *Single Pile and Pile Groups under Lateral Loading*; CRC Press: Boca Raton, FL, USA, 2010.

44. Manoukas, G.; Athanatopoulou, A.; Avramidis, I. Multimode pushover analysis for asymmetric buildings under biaxial seismic excitation based on a new concept of the equivalent single degree of freedom system. *Soil Dyn. Earthq. Eng.* **2012**, *38*, 88–96. [CrossRef]

45. Hwang, H.; Jernigan, J.B.; Lin, Y.W. Evaluation of Seismic Damage to Memphis Bridges and Highway Systems. *J. Bridge Eng.* **2000**, *5*, 322–330. [CrossRef]